Multiscale Computations of Fluid Flows Using an Adaptive Wavelet Method

By

D. Wirasaet, S. Paolucci, and J.M. Powers

Department of Aerospace and Mechanical Engineering
University of Notre Dame, IN 46556

8th World Congress on Computational Mechanics, Venice, Italy, June 30-July 5, 2008

Acknowledge NASA for partial support

Introduction

- ☞ Solutions of many physical problems, formulated as PDEs, may contain sharp local variations in space, whose location may vary with time, in otherwise smooth solutions.
- ☞ Since high resolution is needed to resolve such features, accurate numerical simulations using uniform grids require a large number of **d**egrees **o**f **f**reedoms (DOFs).
- ☞ The number of DOFs for a uniform grid discretization is $O(N^d)$ for problems in d spatial dimensions.
- ☞ To reduce the DOFs required, while maintaining solution accuracy, adaptive discretization becomes necessary.
- ☞ Such task may be accomplished by use of AMR or adaptive FEM, where the refinement is based upon some error estimators/indicators.
- ☞ Alternatively, we tackle such task by using an adaptive wavelet method. The method makes use of a wavelet multiscale basis in the design of the refinement strategy.

Wavelet Approximation in Domain $[0,1]^d$

Approximation of $u(\mathbf{x})$ by the interpolating wavelet, a multiscale basis, on $[0,1]^d$ is given by

$$u(\mathbf{x}) \approx u^J(\mathbf{x}) = \sum_{\mathbf{k}} u_{J_0,\mathbf{k}} \Phi_{J_0,\mathbf{k}}(\mathbf{x}) + \sum_{j=J_0}^{J-1} \sum_{\boldsymbol{\lambda}} d_{j,\boldsymbol{\lambda}} \Psi_{j,\boldsymbol{\lambda}}(\mathbf{x}),$$

where $(\mathbf{x}, \mathbf{k}) \in \mathbf{R}^d$, $\boldsymbol{\lambda} = (\mathbf{e}, \mathbf{k})$, and $\Psi_{j,\boldsymbol{\lambda}}(\mathbf{x}) \equiv \Psi^{\mathbf{e}}_{j,\mathbf{k}}(\mathbf{x})$.

- Scaling function:

$$\Phi_{j,\mathbf{k}}(\mathbf{x}) = \prod_{i=1}^{d} \phi_{j,\mathbf{k}}(x_i), \; k_i \in \kappa_j^0,$$

- Wavelet function:

$$\Psi^{\mathbf{e}}_{j,\mathbf{k}}(\mathbf{x}) = \prod_{i=1}^{d} \psi^{e_i}_{j,\mathbf{k}}(x_i), \; k_i \in \kappa_j^{e_i},$$

where $\mathbf{e} \in \{0,1\}^d \setminus \mathbf{0}$, $\psi^0_{j,k}(x) \equiv \phi_{j,k}(x)$ and $\psi^1_{j,k}(x) \equiv \psi_{j,k}(x)$, and $\kappa_j^0 = \{0, \ldots, 2^j\}$ and $\kappa_j^1 = \{0, \ldots, 2^j - 1\}$.

1-D Interpolating Scaling Function and Wavelet

Some properties of $\phi_{j,k}$ and $\psi_{j,k}$ of order p ($p \in \mathbf{N}$, even):

- ☞ $\phi_{j,k}$ is defined through $\phi(2^j x - k)$ where $\phi(x) = \int \varphi_p(y)\varphi_p(y-x)dy$, the auto-correlation of the Daubechies scaling function $\varphi_p(x)$.
- ☞ The support of $\phi_{j,k}$ is compact, *i.e.* $\text{supp}\{\phi_{j,k}\} \sim |O(2^{-j})|$.
- ☞ $\phi_{j,k}(x_{j,n} = n2^{-j}) = \delta_{k,n}$, *i.e.* satisfies the *interpolation property.*
- ☞ $\psi_{j,k} = \phi_{j+1,2k+1}$.
- ☞ $\text{span}\{\phi_{j,k}\} = \text{span}\{\{\phi_{j-1,k}\}, \{\psi_{j-1,k}\}\}$.
- ☞ $\{1, x, \cdots, x^{p-1}\}$, for $x \in [0,1]$, can be written as a linear combination of $\{\phi_{j,k},\ k = 0, \cdots, 2^j\}$.
- ☞ $\{\{\phi_{J_0,k}\}, \{\psi_{j,k}\}_{j=J_0}^{\infty}\}$ forms a basis of a continuous 1-D function on the unit interval $[0,1]$.

Wavelet Amplitudes

• Wavelet amplitude, $|d_{j,\boldsymbol{\lambda}}|$, measures the approximation error of $f(\mathbf{x})$ by a local polynomial approximation at the point $\mathbf{x}_{j,\boldsymbol{\lambda}}$.

• In other words, wavelet amplitudes, $d_{j,\boldsymbol{\lambda}}$, indicate the local regularity of a function.

Example: Consider $u(x, y) = 0.2/(|0.4 - x^2 - y^2| + 0.2)$

$AFWT(u)$

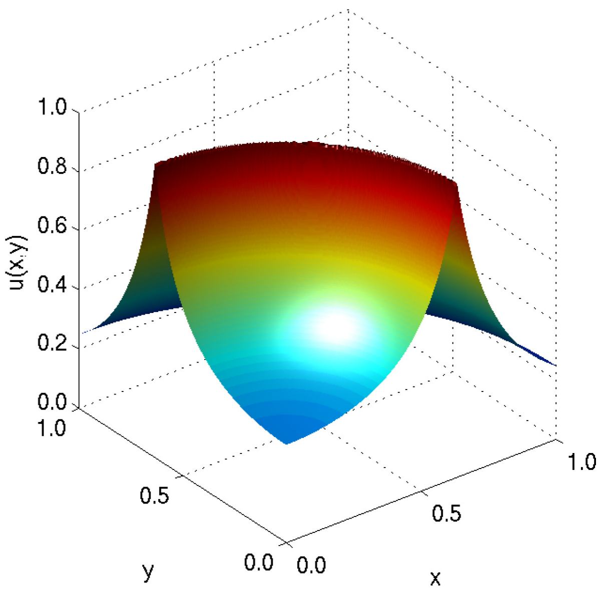

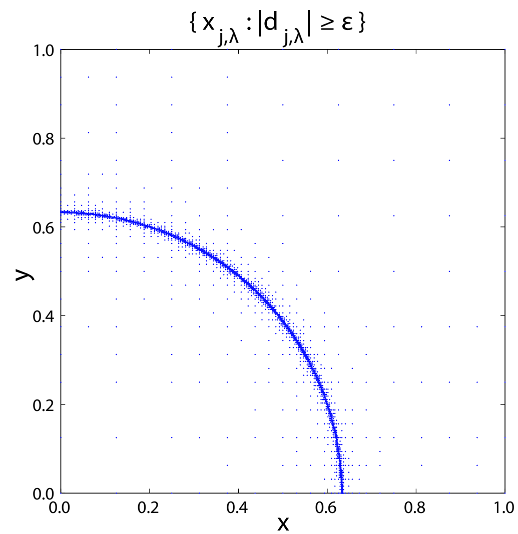

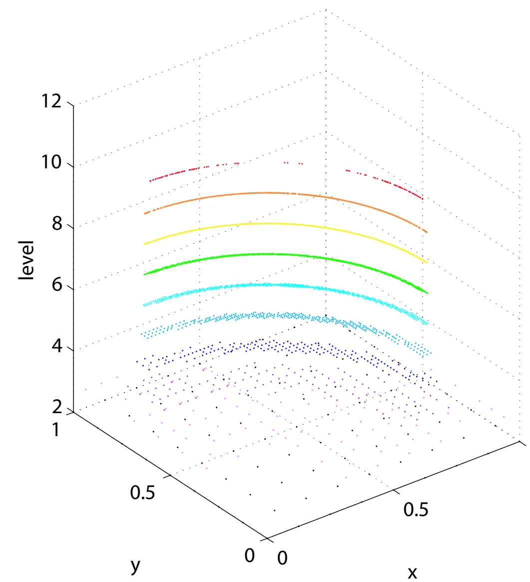

Grid points correspond to wavelet amplitudes that are larger than $\varepsilon = 5 \times 10^{-3}$.

Sparse Wavelet Representation (SWR) and Irregular Sparse Grid

☞ For a given threshold parameter ε, the multiscale approximation of a function $u(\mathbf{x})$ can be written as

$$u^J(\mathbf{x}) = \sum_{\mathbf{k}} u_{J_0,\mathbf{k}} \Phi_{J_0,\mathbf{k}}(\mathbf{x}) + \sum_{j=J_0}^{J-1} \sum_{\{\boldsymbol{\lambda} \,:\, |d_{j,\boldsymbol{\lambda}}| \geq \varepsilon\}} d_{j,\boldsymbol{\lambda}} \Psi_{j,\boldsymbol{\lambda}}(\mathbf{x}) + \underbrace{\sum_{j=J_0}^{J-1} \sum_{\{\boldsymbol{\lambda} \,:\, |d_{j,\boldsymbol{\lambda}}| < \varepsilon\}} d_{j,\boldsymbol{\lambda}} \Psi_{j,\boldsymbol{\lambda}}(\mathbf{x})}_{R_\varepsilon^J}.$$

☞ The Sparse Wavelet Representation (SWR) is obtained by discarding the term R_ε^J:

$$u_\varepsilon^J(\mathbf{x}) = \sum_{\mathbf{k}} u_{J_0,\mathbf{k}} \Phi_{J_0,\mathbf{k}}(\mathbf{x}) + \sum_{j=J_0}^{J-1} \sum_{\{\boldsymbol{\lambda} \,:\, |d_{j,\boldsymbol{\lambda}}| \geq \varepsilon\}} d_{j,\boldsymbol{\lambda}} \Psi_{j,\boldsymbol{\lambda}}(\mathbf{x}).$$

SWR and Irregular Sparse Grid (continued)

- In the context of interpolating wavelets, each basis function is associated with one dyadic grid point, *i.e.*

$$\Phi_{j,\mathbf{k}}(\mathbf{x}) \quad \text{with} \quad \mathbf{x}_{j,\mathbf{k}} = (k_1 2^{-j}, \ldots, k_d 2^{-j}),$$
$$\Psi_{j,\boldsymbol{\lambda}}(\mathbf{x}) \quad \text{with} \quad \mathbf{x}_{j,\boldsymbol{\lambda}} = \mathbf{x}_{j+1,2\mathbf{k}+\mathbf{e}}.$$

- Thus, for a given SWR, one can establish an associated grid of irregular points

$$\boldsymbol{\mathcal{V}} = \{\mathbf{x}_{J_0,\mathbf{k}}, \cup_{j\geq J_0} \mathbf{x}_{j,\boldsymbol{\lambda}} \ : \ \boldsymbol{\lambda} \in \boldsymbol{\Lambda}_j\}, \quad \boldsymbol{\Lambda}_j = \{\boldsymbol{\lambda} \ : \ |d_{j,\boldsymbol{\lambda}}| \geq \varepsilon\}.$$

- Due to the interpolation property of the basis, there exists a fast wavelet transform ($AFWT$), with $O(N)$ operations, $N = \dim\{\boldsymbol{\mathcal{V}}\}$, that maps function values on the irregular grid $\boldsymbol{\mathcal{V}}$ to associated wavelet coefficients and *vice-versa*:

$$AFWT(\{u(\mathbf{x}) \ : \ \mathbf{x} \in \boldsymbol{\mathcal{V}}\}) \rightarrow \mathcal{D} = \{\{u_{J_0,\mathbf{k}}\}, \{d_{j,\boldsymbol{\lambda}}, \ \boldsymbol{\lambda} \in \boldsymbol{\Lambda}_j\}\}.$$

SWR and Irregular Sparse grid (continued)

☞ Provided that the function $u(\mathbf{x})$ is continuous, the error in the SWR $u_\varepsilon^J(\mathbf{x})$ is bounded by

$$\|u - u_\varepsilon^J\|_\infty \leq C_1\, \varepsilon.$$

☞ Furthermore, for a function that is sufficiently smooth, the number of basis functions $N = \dim\{u_\varepsilon^J\}$ required for a given ε satisfies

$$N \leq C_2\, \varepsilon^{-d/p},$$

so that we also have

$$\|u - u_\varepsilon^J\|_\infty \leq C_2\, N^{-p/d}.$$

Dynamically Adaptive Algorithm for Solving Time-dependent PDEs

Numerical algorithm:

$$
\begin{aligned}
\frac{\partial u}{\partial t} &= F(t, u, u_x, u_{xx}, \ldots) \\
\Longrightarrow \mathcal{A}^{m+1} u^{m+1} &= \mathcal{F}^{m+1}(t^{m+1}, t^{m-q}, u^{m-q}, \ldots), q = 0, \ldots, m \quad (1)
\end{aligned}
$$

① Solve (1) to obtain the approximate solution u^{m+1} on the irregular grid $\boldsymbol{\mathcal{V}}^m$ by using the solution from the previous time step, u^m, as initial condition.

② Obtain the new sparse grid, $\boldsymbol{\mathcal{V}}^{m+1}$, based on the thresholding of the magnitudes of wavelet amplitudes of the new solution, u^{m+1}.

③ Assign $\boldsymbol{\mathcal{V}}^{m+1} \rightarrow \boldsymbol{\mathcal{V}}^m$ and $u^{m+1-q} \rightarrow u^{m-q}$, $q = 0, \ldots, m$ and go back to step ①.

Note: The initial sparse grid set, $\boldsymbol{\mathcal{V}}^0$, is obtained from initial conditions.

Grid Adaption Strategy

- In each refinement step, determine the *essential* grid points, which are points whose associated wavelet amplitudes are larger than the threshold parameter ε:

$$\widehat{\boldsymbol{\mathcal{V}}}_e = \{\mathbf{x}_{j,\boldsymbol{\lambda}} \;:\; j \geq J_0,\ \boldsymbol{\lambda} \in \boldsymbol{\Lambda}_j,\ |d_{j,\boldsymbol{\lambda}}| \geq \varepsilon\}.$$

- To accommodate the possible advection and sharpening of solution features, we determine the *neighboring* grid points:

$$\widehat{\boldsymbol{\mathcal{V}}}_b = \bigcup_{\{j,\boldsymbol{\lambda}\in\boldsymbol{\Lambda}\}} \mathcal{N}_{j,\boldsymbol{\lambda}},$$

  where $\mathcal{N}_{j,\boldsymbol{\lambda}}$ is the set of neighboring points to $x_{j,\boldsymbol{\lambda}}$.

- The new sparse grid, $\boldsymbol{\mathcal{V}}$, is then given by

$$\boldsymbol{\mathcal{V}} = \{\mathbf{x}_{J_0,\mathbf{k}}\} \cup \widehat{\boldsymbol{\mathcal{V}}}_e \cup \widehat{\boldsymbol{\mathcal{V}}}_b.$$

Applications to Reactive Compressible Navier-Stokes Equations

Governing Equations (1-D):

$$\frac{\partial \rho}{\partial t} + \frac{\partial}{\partial x}(\rho u) = 0$$

$$\frac{\partial}{\partial t}(\rho u) + \frac{\partial}{\partial x}\left(\rho u^2 + P - \tau\right) = 0$$

$$\frac{\partial}{\partial t}\left(\rho\left(e + \frac{u^2}{2}\right)\right) + \frac{\partial}{\partial x}\left(\rho u\left(e + \frac{u^2}{2}\right) + u(P - \tau) + q\right) = 0$$

$$\frac{\partial}{\partial t}(\rho Y_i) + \frac{\partial}{\partial x}(\rho u Y_i + j_i) = \dot{\omega}_i$$

Applications to Reactive Compressible Navier-Stokes Equations (continued)

Constitutive Equations:

$$P = \rho \Re T \sum_{i=1}^{N} \frac{Y_i}{M_i} \quad \text{(thermal equation of state)}$$

$$e = \sum_{i=1}^{N} Y_i \left(h_i^o + \int_{T_o}^{T} c_{pi}(\hat{T}) d\hat{T} \right) - \frac{P}{\rho} \quad \text{(caloric equation of state)}$$

$$\tau = \frac{4}{3}\mu \frac{\partial u}{\partial x} \quad \text{(Newtonian gas with Stokes' assumption)}$$

$$j_i = -\rho \sum_{j=1}^{N} \mathcal{D}_{ij} \frac{\partial Y_j}{\partial x} \quad \text{(Fick's law)}$$

$$q = -k\frac{\partial T}{\partial x} + \sum_{i=1}^{N} j_i \left(h_i^o + \int_{T_o}^{T} c_{pi}(\hat{T}) d\hat{T} \right) \quad \text{(augmented Fourier's law)}$$

$$\dot{\omega}_i = \sum_{j=1}^{M} a_j T^{\alpha_j} \exp\left(\frac{-E_j}{\Re T} \right) \nu_{ij} M_i \prod_{k=1}^{N} \left(\frac{\rho Y_k}{M_k} \right)^{\nu_{kj}} \quad \text{(reaction rate)}$$

Operator Splitting

System of equations:

$$\mathbf{q}_t(x,t) + \mathbf{f}_x(\mathbf{q}(x,t)) = \mathbf{r}(\mathbf{q}(x,t)),$$

where $\mathbf{q} = \left(\rho, \rho u, \rho\left(e + \frac{u^2}{2}\right), \rho Y_i\right)^T$. Note that $\mathbf{f}$ models convection and diffusion, while $\mathbf{r}$ models the reaction source terms.

Strang splitting:

☞ Inert convection-diffusion integration (AB2):

$$\mathbf{q}_t(x,t) = -\mathbf{f}_x(\mathbf{q}(x,t)) = \mathcal{S}_c(\mathbf{q}(x,t)),$$

☞ Reaction source integration (BD2):

$$\mathbf{q}_t(x,t) = \mathbf{r}(\mathbf{q}(x,t)) = \mathcal{S}_r.$$

☞ Time integration:

$$\mathbf{q}(x, t+\Delta t) = \mathcal{S}_r(\Delta t/2)\mathcal{S}_c(\Delta t)\mathcal{S}_r(\Delta t/2)\mathbf{q}(x,t).$$

Operator Splitting (continued)

The reaction source step

$$\frac{\partial}{\partial t}\begin{pmatrix} \rho \\ \rho u \\ \rho\left(e+\frac{u^2}{2}\right) \\ \rho Y_i \end{pmatrix} = \begin{pmatrix} 0 \\ 0 \\ 0 \\ \omega \end{pmatrix}$$

Reduces to

$$\rho = \rho_o, \qquad u = u_o, \qquad e = e_o, \qquad \frac{\partial Y_i}{\partial t} = \frac{\omega}{\rho_o}.$$

Note:

- ☞ ω has dependency on ρ, e, and Y_i.
- ☞ ODEs for Y_i can be solved pointwise.

Ignition delay problem

Premixed H_2-O_2-Ar in 2/1/7 molar ratio

9 species: H_2, O_2, H, O, OH, H_2O_2, H_2O, HO_2, Ar

37 reactions:

j	Reaction	a_j	β_j	E_j
1	$O_2 + H \to OH + O$	2.00×10^{14}	0.00	70.30
2	$OH + O \to O_2 + H$	1.46×10^{13}	0.00	2.08
3	$H_2 + O \to OH + H$	5.06×10^{4}	2.67	26.30
4	$OH + H \to H_2 + O$	2.24×10^{4}	2.67	18.40
5	$H_2 + OH \to H_2O + H$	1.00×10^{8}	1.60	13.80
6	$H_2O + H \to H_2 + OH$	4.45×10^{8}	1.60	77.13
7	$OH + OH \to H_2O + O$	1.50×10^{9}	1.14	0.42
8	$H_2O + O \to OH + OH$	1.51×10^{10}	1.14	71.64
9	$H + H + M \to H_2 + M$	1.80×10^{18}	-1.00	0.00
10	$H_2 + M \to H + H + M$	6.99×10^{18}	-1.00	436.08
11	$H + OH + M \to H_2O + M$	2.20×10^{22}	-2.00	0.00
12	$H_2O + M \to H + OH + M$	3.80×10^{23}	-2.00	499.41
13	$O + O + M \to O_2 + M$	2.90×10^{17}	-1.00	0.00
14	$O_2 + M \to O + O + M$	6.81×10^{18}	-1.00	496.41
15	$H + O_2 + M \to HO_2 + M$	2.30×10^{18}	-0.80	0.00
16	$HO_2 + M \to H + O_2 + M$	3.26×10^{18}	-0.80	195.88
17	$HO_2 + H \to OH + OH$	1.50×10^{14}	0.00	4.20
18	$OH + OH \to HO_2 + H$	1.33×10^{13}	0.00	168.30
19	$HO_2 + H \to H_2 + O_2$	2.50×10^{13}	0.00	2.90

j	Reaction	a_j	β_j	E_j
20	$H_2 + O_2 \to HO_2 + H$	6.84×10^{13}	0.00	243.10
21	$HO_2 + H \to H_2O + O$	3.00×10^{13}	0.00	7.20
22	$H_2O + O \to HO_2 + H$	2.67×10^{13}	0.00	242.52
23	$HO_2 + O \to OH + O_2$	1.80×10^{13}	0.00	-1.70
24	$OH + O_2 \to HO_2 + O$	2.18×10^{13}	0.00	230.61
25	$HO_2 + OH \to H_2O + O_2$	6.00×10^{13}	0.00	0.00
26	$H_2O + O_2 \to HO_2 + OH$	7.31×10^{14}	0.00	303.53
27	$HO_2 + HO_2 \to H_2O_2 + O_2$	2.50×10^{11}	0.00	-5.20
28	$OH + OH + M \to H_2O_2 + M$	3.25×10^{22}	-2.00	0.00
29	$H_2O_2 + M \to OH + OH + M$	2.10×10^{24}	-2.00	206.80
30	$H_2O_2 + H \to H_2 + HO_2$	1.70×10^{12}	0.00	15.70
31	$H_2 + HO_2 \to H_2O_2 + H$	1.15×10^{12}	0.00	80.88
32	$H_2O_2 + H \to H_2O + OH$	1.00×10^{13}	0.00	15.00
33	$H_2O + OH \to H_2O_2 + H$	2.67×10^{12}	0.00	307.51
34	$H_2O_2 + O \to OH + HO_2$	2.80×10^{13}	0.00	26.80
35	$OH + HO_2 \to H_2O_2 + O$	8.40×10^{12}	0.00	84.09
36	$H_2O_2 + OH \to H_2O + HO_2$	5.40×10^{12}	0.00	4.20
37	$H_2O + HO_2 \to H_2O_2 + OH$	1.63×10^{13}	0.00	132.71

Table Nine-species, 37-step reaction mechanism for a hydrogen–oxygen–argon mixture [25] with corrected f_{H_2} from [3], also utilized by Fedkiw *et al* [16]. Units of a_j are in appropriate combinations of cm, mol, s and K so that $\dot{\omega}_i$ has units of mol cm^{-3} s^{-1}; units of E_j are kJ mol^{-1}. Third-body collision efficiencies with M are $f_{H_2} = 1.00$, $f_{O_2} = 0.35$ and $f_{H_2O} = 6.5$.

$t = 230\ \mu s$

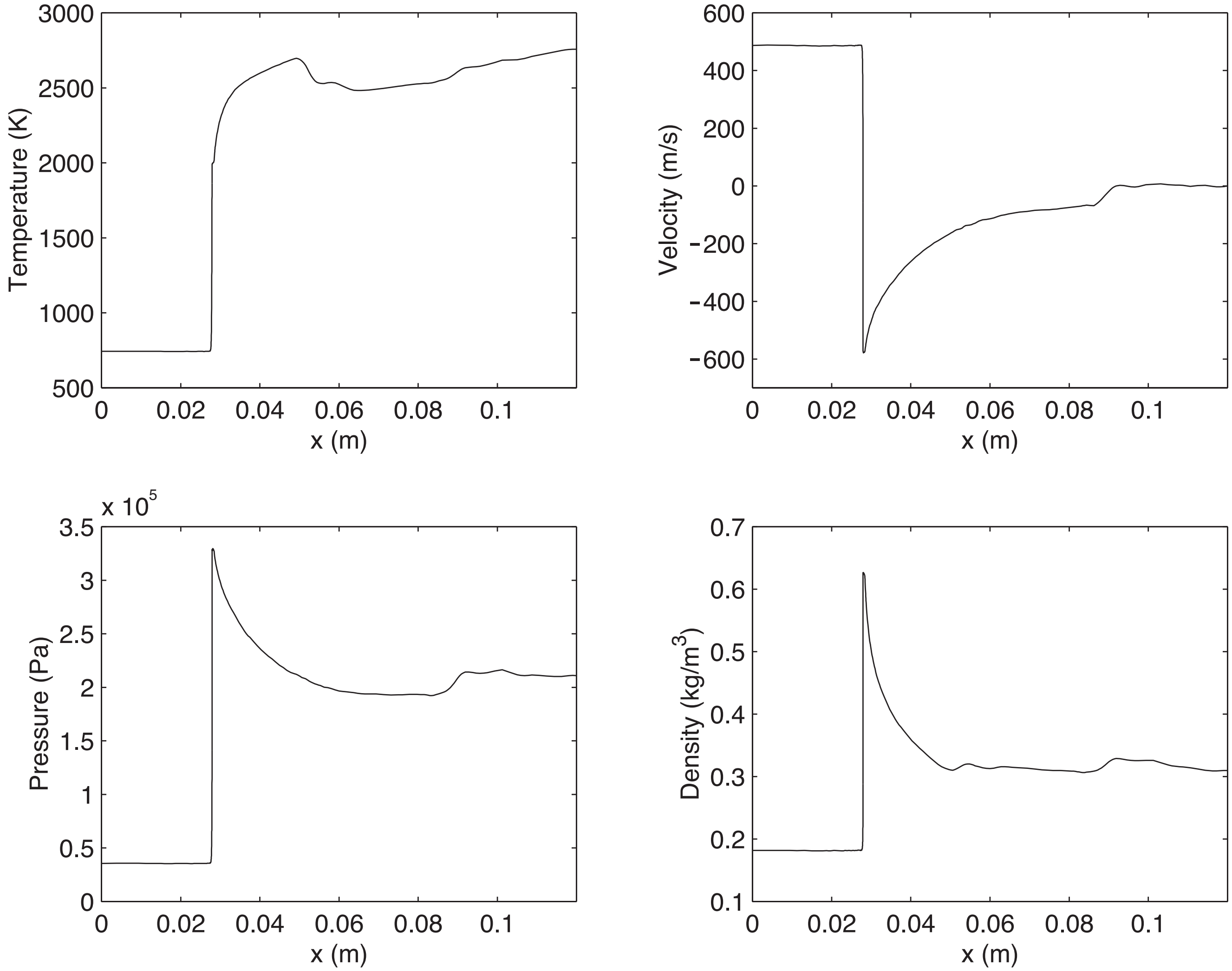

Temperature (K)
3000
2500
2000
1500
1000
500
Velocity (m/s)
600
400
200
0
-200
-400
-600
x 10^5
Pressure (Pa)
3.5
3
2.5
2
1.5
1
0.5
0
Density (kg/m^3)
0.7
0.6
0.5
0.4
0.3
0.2
0.1
0
0.02
0.04
0.06
0.08
0.1
x (m)

$t = 180, 190, 200, 230\ \mu s$

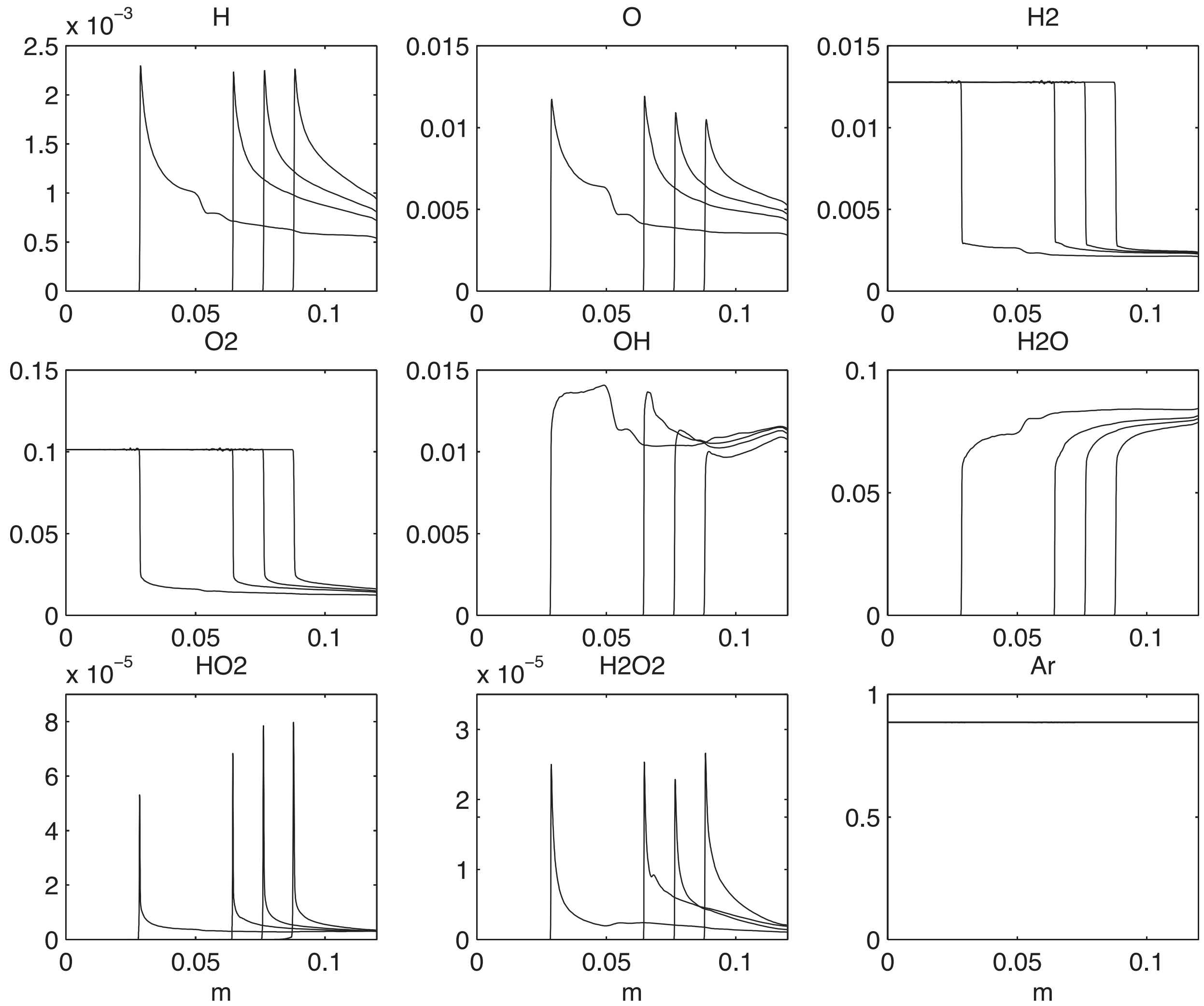

Large and small scale structures at $t = 230\ \mu s$

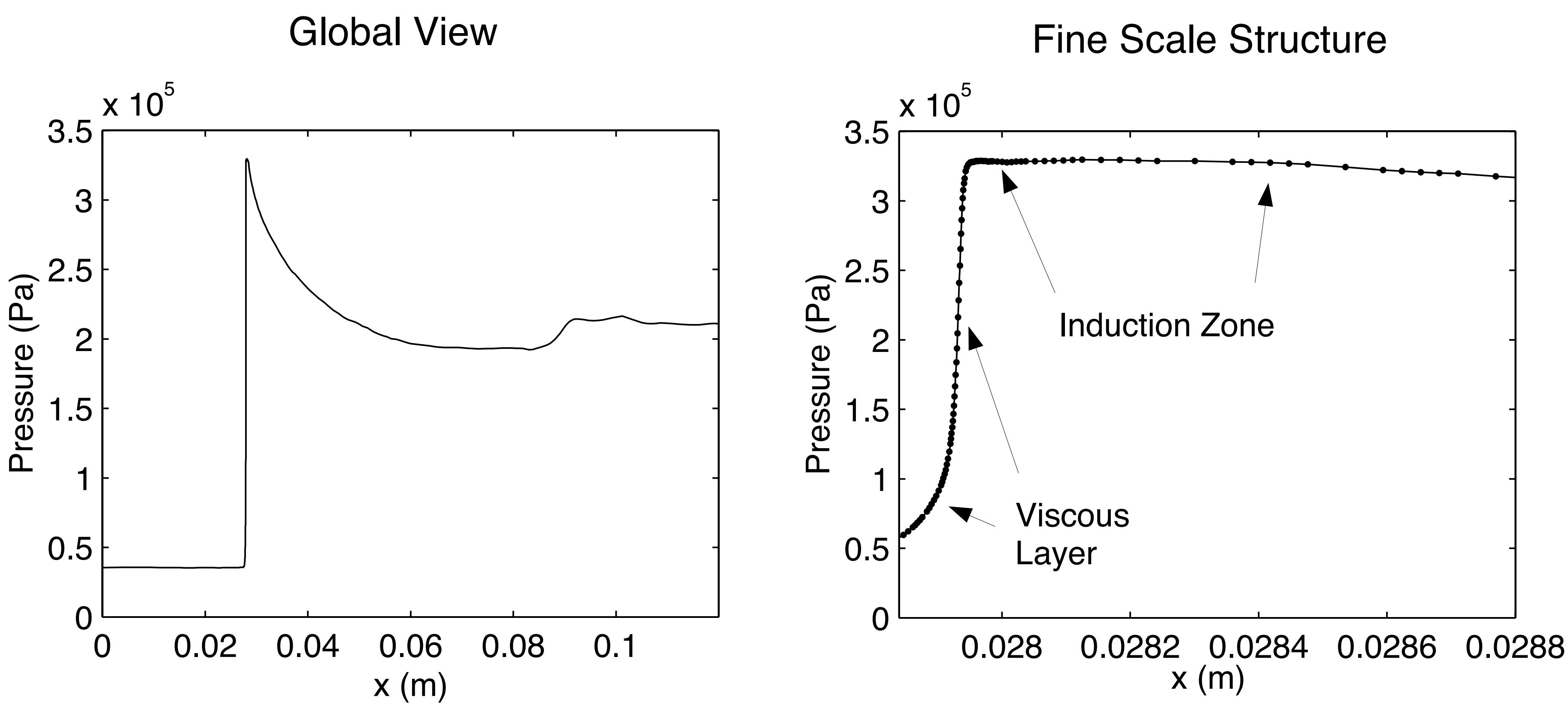

Instantaneous distribution of collocation points

Used at most 300 points and 15 scale levels

$t = 180$ μs two-shocks and at $t = 230$ μs one-shock (detonation).

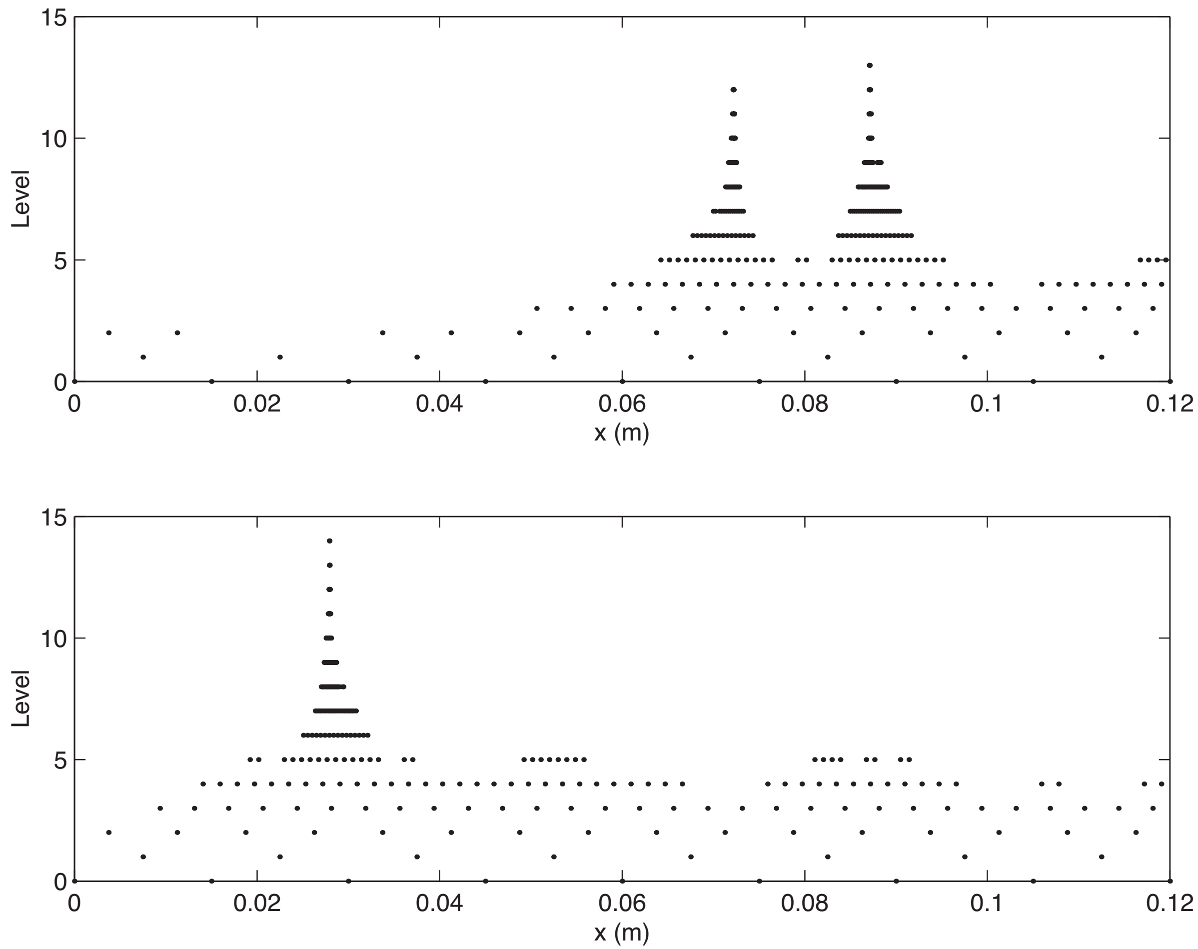

Applications to Incompressible Navier-Stokes Equations

Governing Equations:

$$
\begin{aligned}
\nabla \cdot \mathbf{u} &= 0, \\
\frac{\partial \mathbf{u}}{\partial t} + \mathbf{u} \cdot \nabla \mathbf{u} &= -\nabla p + \frac{1}{Re} \nabla^2 \mathbf{u} - \frac{Gr}{Re^2} T \ \mathbf{n}, \\
\frac{\partial T}{\partial t} + \mathbf{u} \cdot \nabla T &= \frac{1}{RePr} \nabla^2 T,
\end{aligned}
$$

with appropriate boundary and initial conditions.

- ☞ $\mathbf{n}$ is the unit vector in the direction of gravity.
- ☞ $Re = UL/\nu$, $Gr = g\beta \Delta T L^3/\nu^2$, and $Pr = \nu/\alpha$.

Note: L, U, L/U, and ΔT are reference length, velocity, time, and temperature scales, and $T = (T^* - T_r)/\Delta T$.

2nd order Fractional Step Method

☞ Step ①. Compute the temperature field:

$$\frac{T^{m+1}-T^m}{\Delta t}+\frac{1}{2}(\widetilde{\mathbf{u}}\cdot\nabla)(T^{m+1}+T^m)=\frac{1}{2RePr}\nabla^2(T^{m+1}+T^m),$$

where $\widetilde{\mathbf{u}}=(1+r)\mathbf{u}^m-r\mathbf{u}^{m-1}$ with $r=\dfrac{\Delta\tau}{\Delta t}$, $\Delta t=t^{m+1}-t^m$, $\Delta\tau=t^m-t^{m-1}$.

☞ Step ②. Solve for the intermediate velocity $\widehat{\mathbf{u}}$:

$$\frac{\widehat{\mathbf{u}}-\mathbf{u}^m}{\Delta t}+\frac{1}{2}(\widetilde{\mathbf{u}}\cdot\nabla\widehat{\mathbf{u}}+\mathbf{u}^m)\cdot\nabla\mathbf{u}^m=-\nabla\tilde{p}+\frac{1}{2Re}\nabla^2(\widehat{\mathbf{u}}+\mathbf{u}^m)-\frac{Gr\mathbf{n}}{2Re^2}(T^{m+1}+T^m).$$

☞ Step ③. Determine the true velocity $\mathbf{u}^{m+1}$:

$$\left.\begin{aligned}&\mathbf{u}^{m+1}-\widehat{\mathbf{u}}=-\Delta t\ \nabla\phi,\\ &\nabla\cdot\mathbf{u}^{m+1}=0,\end{aligned}\right\}\Longrightarrow\quad\nabla^2\phi=(\nabla\cdot\widehat{\mathbf{u}})/\Delta t.$$

☞ Step ④. When needed, compute the pressure field:

$$p^{m+1}=\widetilde{p}+\phi-1/2\sqrt{Ra/Pr}\ \Delta t\nabla^2\phi.$$

2-D Differentially Heated Cavity

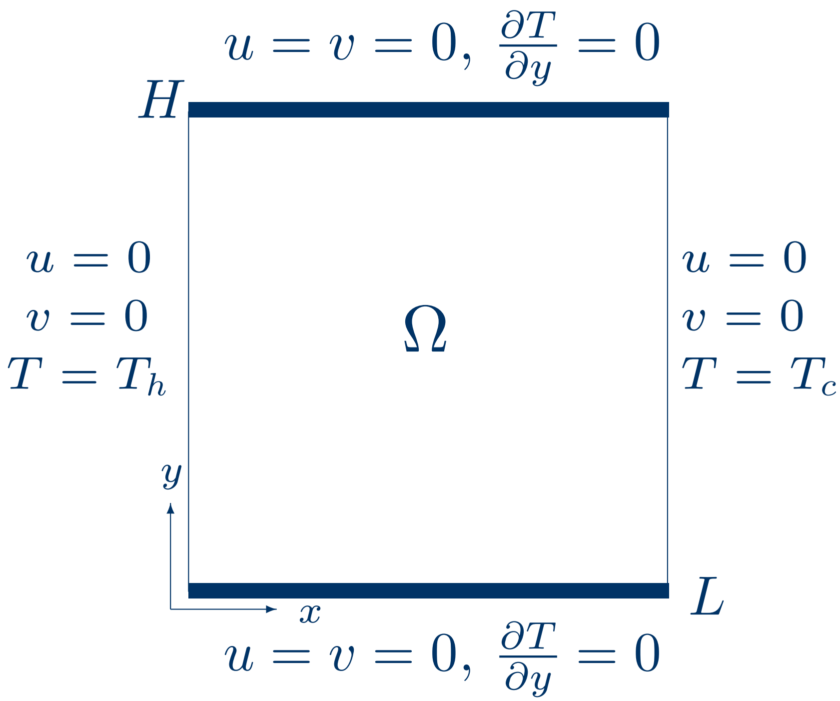

- $\Delta T \equiv T_h - T_c$ and $T_r \equiv (T_h + T_c)/2$, $T_h > T_c$.
- H, $U = \sqrt{\beta g \Delta T H}$, ΔT, and H/U are used as reference length, velocity, temperature, and time scales.
- $Re^2 = Gr = Ra/Pr$, where the Rayleigh number $Ra = \beta g \Delta T H^3/\nu^2$.

- For a square cavity, $H = L$, $\Omega = (0,1)^2$ and BCs are given by

$$\mathbf{u} = \mathbf{0}, \quad \text{on} \quad x = 0,\ 1 \quad \text{and} \quad y = 0,\ 1,$$
$$T = \frac{1}{2} - x, \quad \text{on} \quad x = 0, 1 \quad \text{and} \quad \frac{\partial T}{\partial y} = 0 \quad \text{on} \quad y = 0,\ 1.$$

Numerical Simulations

- The adaptive wavelet method is applied to compute the flow of air $(Pr = 0.71)$ in a square cavity for $Ra = 10^6$ to 5×10^8.

- In each case, the initial condition is chosen to be that of the pure conducting quiescent state $(i.e.\ T(\mathbf{x}, 0) = 1/2 - x$ and $\mathbf{u}(\mathbf{x}, 0) = \mathbf{0})$.

- The steady state, if it exists, is reached through unsteady integration in time satisfying

$$\frac{\|f^{m+1} - f^m\|_{\boldsymbol{\mathcal{V}}^m,\infty}}{\|f^{m+1}\|_{\boldsymbol{\mathcal{V}}^m,\infty}} \leq 5 \times 10^{-5},$$

where $f = \{\mathbf{u}, T\}$.

Parameters of the adaptive method:

Interpolating wavelet	: $p = 6$ with $n = 4$.
Resolution	: $J_0 = 3,\ J - J_0 = 6$.
Threshold	: $\boldsymbol{\varepsilon} = \mathbf{10^{-3}}$ and $\mathbf{5} \times \mathbf{10^{-3}}$.

Results for $Ra = 10^8$

Steady state solution for $\boldsymbol{\varepsilon = 10^{-3}}$, $N = 8791$

Velocity & Temperature

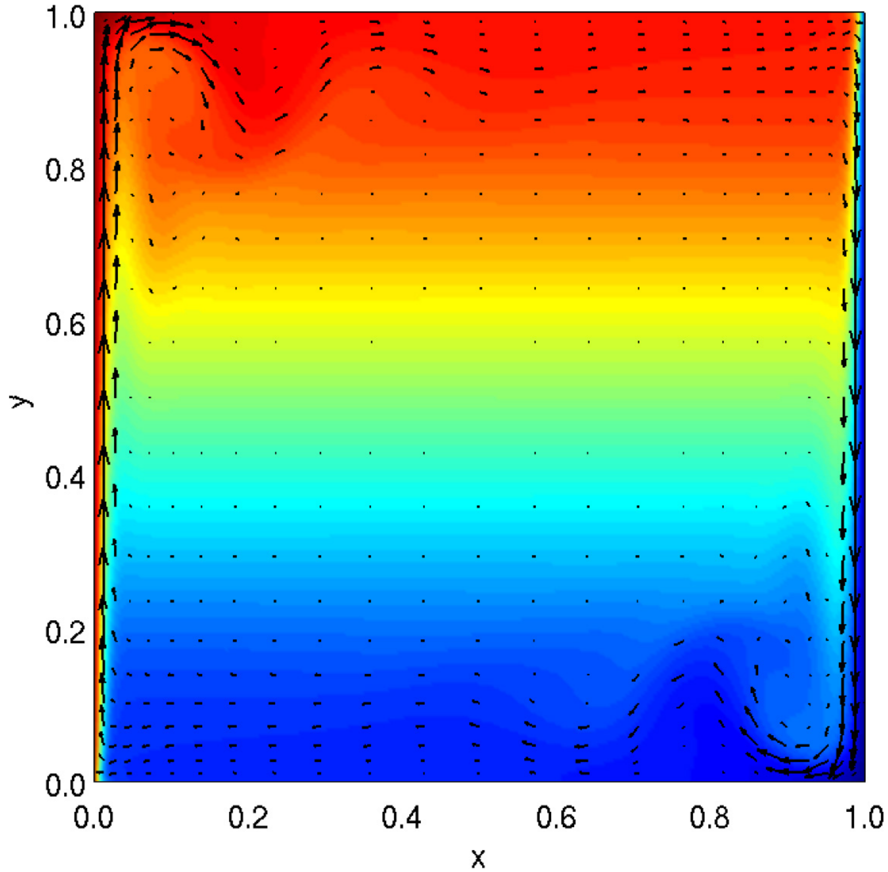

Adaptive Grid

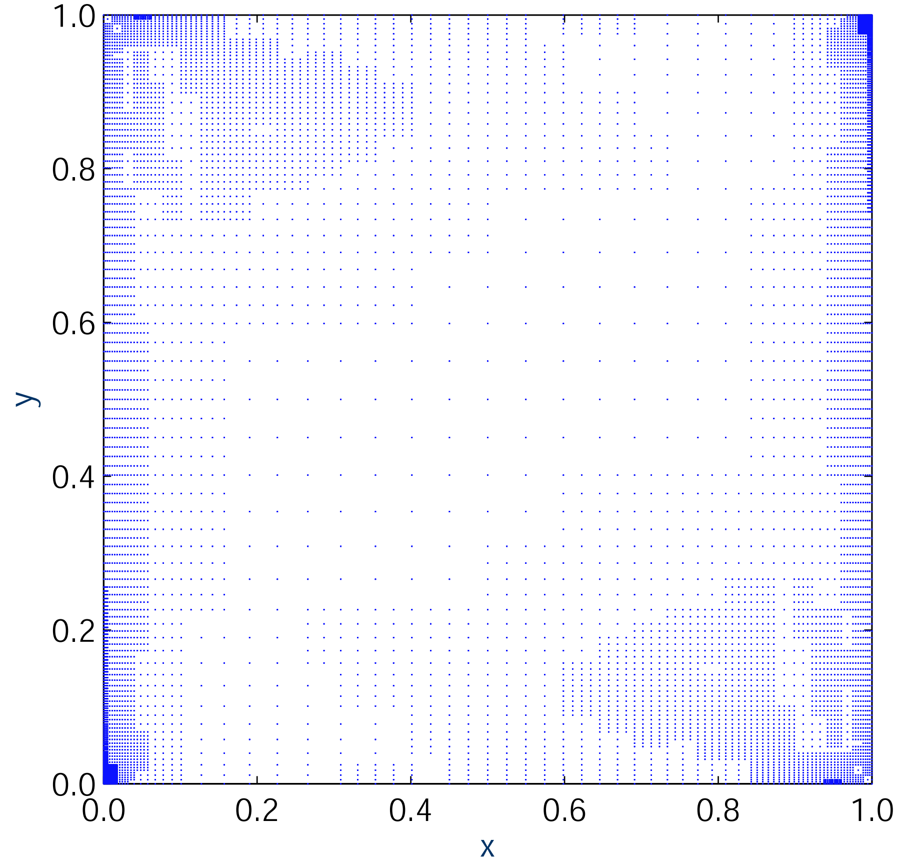

Results for $Ra = 10^8$
Evolution of DOFs

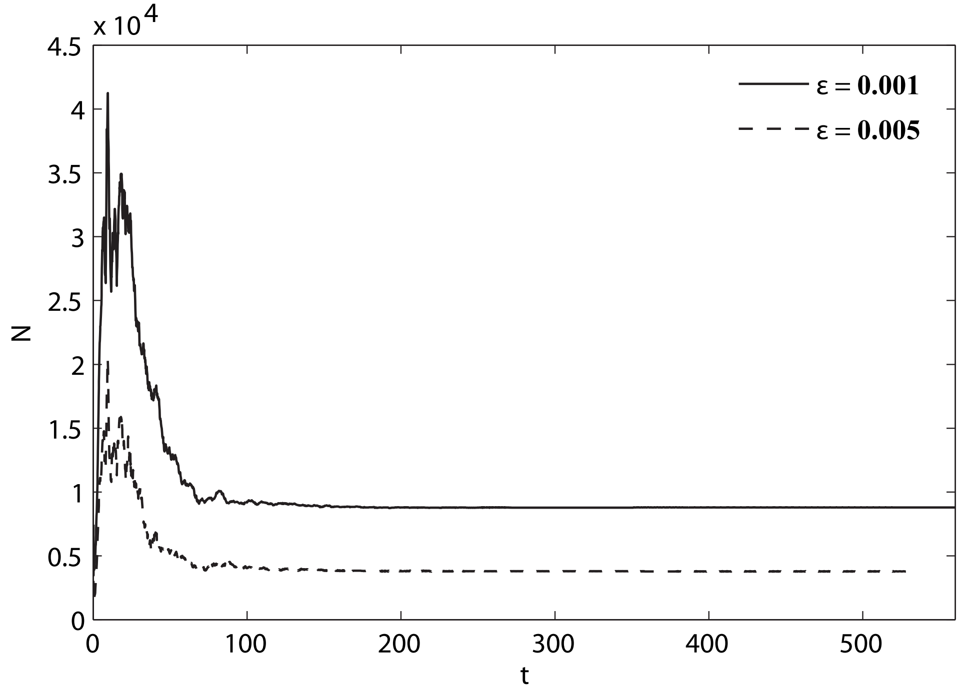

☞ In the early part of the simulation, the solution is quite complicated and requires a relatively large number of DOFs.

☞ As ε is decreased, the number of DOFs, N, generated by algorithm increases automatically.

$Ra = 5 \times 10^8$ AT EARLY TIME WITH $\varepsilon = \{10^{-3}, 4 \times 10^{-3}, 4 \times 10^{-3}\}$

$t = 33.33, N = 42906$

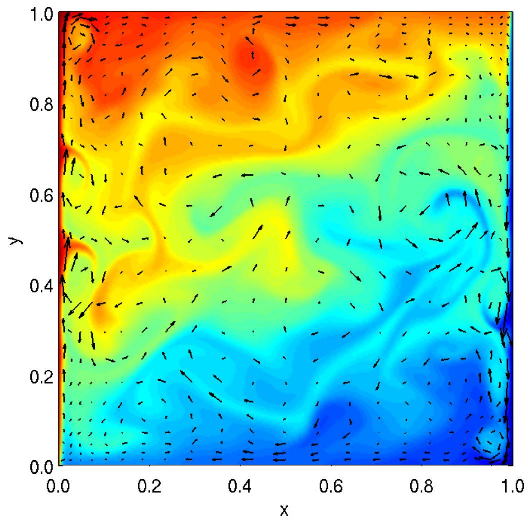

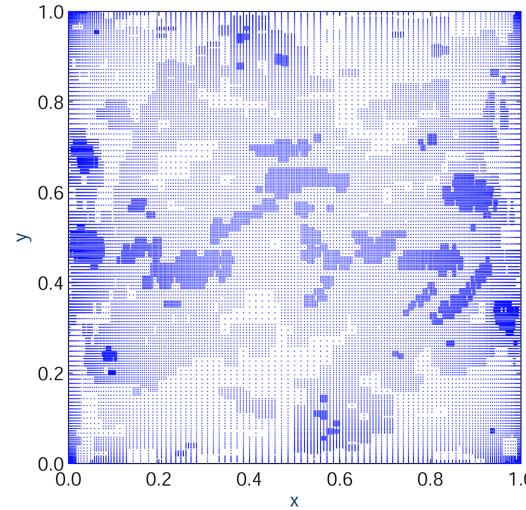

$t = 55.55, N = 29335$

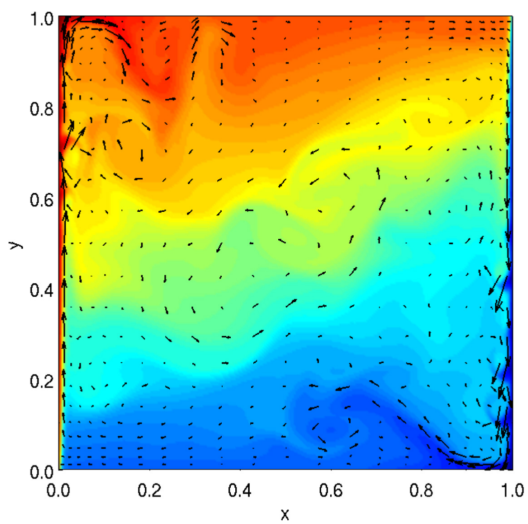

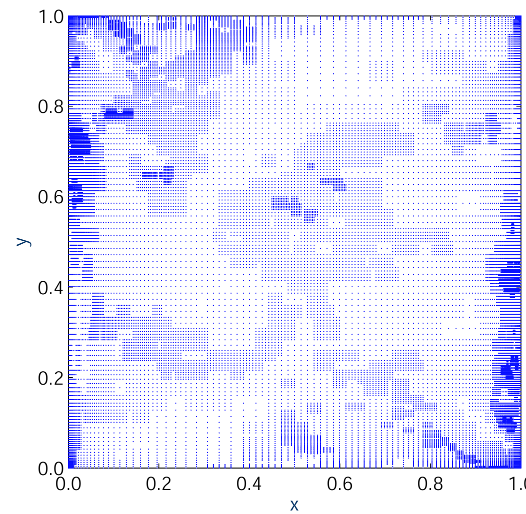

VELOCITY & TEMPERATURE

ADAPTIVE GRID

$Ra = 5 \times 10^8$ AFTER LONG TIME WITH $\varepsilon = \{10^{-3}, 4 \times 10^{-3}, 4 \times 10^{-3}\}$

$t = 418.89,\ N = 9897$

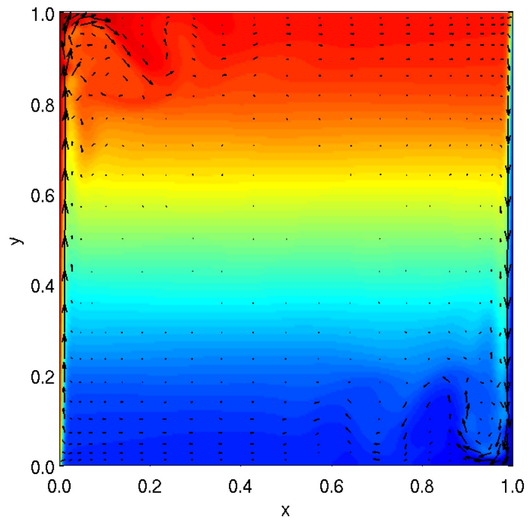

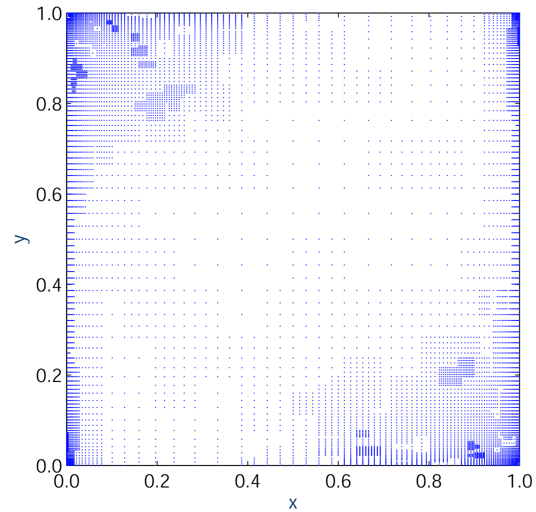

$t = 439.72,\ N = 9281$

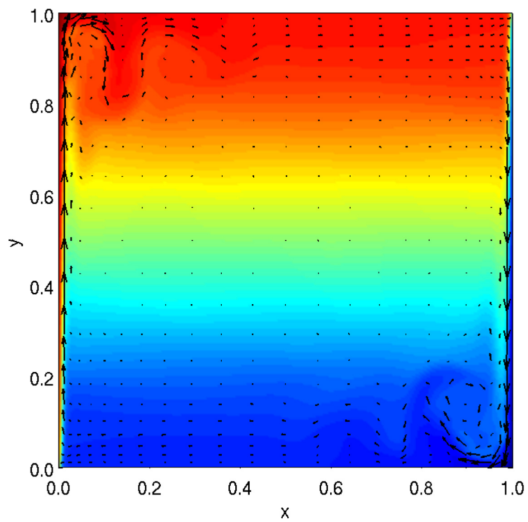

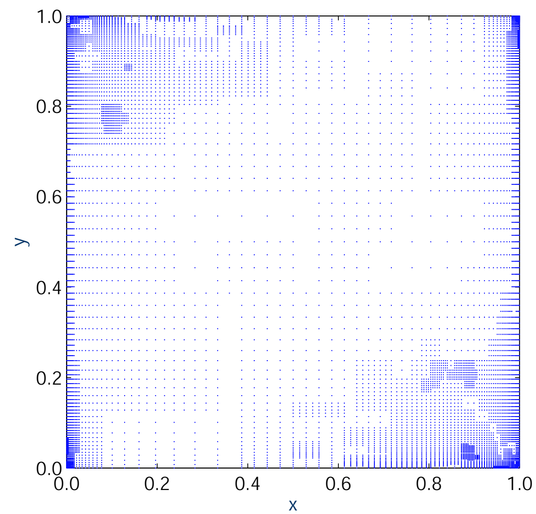

VELOCITY & TEMPERATURE

ADAPTIVE GRID

Results for $Ra = 5 \times 10^8$

Evolution of DOFs required

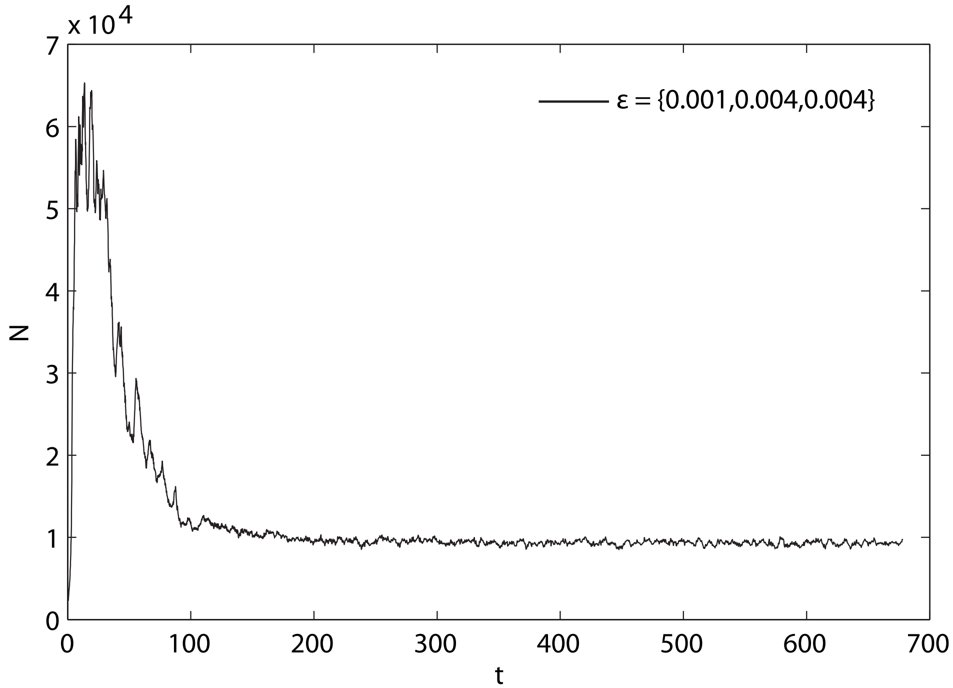

- ☞ In the early part of simulation, the solution is quite complicated and requires a relatively large number of DOF.
- ☞ The flow evolves to produce an approximately stratified and quiescent region in the core of the cavity, with a required number of DOF that is substantially smaller.

Conclusions

- An adaptive wavelet algorithm for solving PDEs in d-dimensions has been described. The algorithm is based on d-dimensional interpolating wavelets.

- Numerical results indicate that the adaptive algorithm behaves approximately like

$$\|u_{exact} - u_{\varepsilon}^{J}\|_{\boldsymbol{\mathcal{V}},\infty} = O(\boldsymbol{\varepsilon}^{\min(p-2,n)/p}), \qquad N = O(\boldsymbol{\varepsilon}^{-d/p}).$$

- The method has been applied to solve compressible and incompressible flows described by the Navier-Stokes equations in primitive variables in 1-D, 2-D, and 3-D geometries.

- Solutions obtained agree well with accurate benchmark results (obtained with much larger number of DOFs) available in the literature.